Quantum Electronics **36** (9) 825 – 834 (2006)

PACS numbers: 42.65.Jx; 32.80.Fb; 32.80.Rm
DOI: 10.1070/QE2006v036n09ABEH013233

Features of the femtosecond pulse propagation in air

A.D. Balashov, A.Kh. Pergament

***Abstract*. The features of propagation of femtosecond laser pulses in the atmosphere are studied by numerical methods. The type of propagation is determined by the relation between processes of multiphoton ionisation and multiple small-scale self-focusing (filamentation). It is found that the process develops step by step and filamentation occurs without the pulse energy loss until the intensity threshold is achieved. After the achievement of the threshold, ionisation losses appear which are accompanied by the defocusing action of the electron plasma resulting in the intensity decrease. When the intensity becomes lower than the ionisation threshold, self-focusing can again appear. The characteristic features of the final stage of filamentation can be explained by the Bespalov – Talanov theory. By using the time-averaged equations and parallel methods, a program complex is developed for qualitative simulations of the propagation of high-power laser pulses over long distances.**

Keywords: *femtosecond pulses, filamentation, interaction of high-power radiation with a medium.*

1. Introduction

Among the possible propagation regimes of laser radiation in a nonlinear medium, the propagation of a high-power femtosecond pulse in air attracts considerable interest at present and can be used for remote sensing, in microphotonics, and for remote control of an electric discharge [1]. The first experiments on the propagation of femtosecond laser pulses over long distances were performed in the mid-1990s [2 – 4]. In these experiments, IR lasers were used which emitted ~ 100 fs pulses with power exceeding the critical value, i.e., the power sufficient for pulse self-focusing [5]. The decomposition of the laser beam into narrow filaments of length of a few meters was observed, the number of produced filaments being dependent on the pulse power.

In this paper, we describe in detail the filamentation process: the reasons for its appearance, the development and its influence on the laser pulse profile. Our model takes into account the effect of ionisation, which allows us to limit the characteristic spatial scale. The pulse intensity increases during self-focusing and its duration decreases, however, no collapse occurs due to the defocusing action of the electron plasma produced upon multiphoton ionisation of air molecules. As a result, the maximum radiation intensity in a filament does not exceed 10^{14} W cm^{-2} for IR pulses. In the region of the maximum intensity, a focus moving along the propagation direction of the pulse is observed. The trace of the focus is called a filament and the process of formation of such structures is called filamentation.

It was shown in [6] that the power of a solitary pulse monotonically decreases down to the critical value. The pulse energy (and power) decreases due to multiphoton ionisation, and the initial shape of the pulse is such that the peak intensity above the threshold is preserved until the achievement of the critical power.

The specific features of filamentation are caused by the Bespalov – Talanov instability, which gives rise to small-scale self-focusing, and by the defocusing action of the electron plasma produced upon multiphoton ionisation. Self-focusing begins when the beam power exceeds the critical value [5], whereas multiphoton ionisation begins when the intensity exceeds the threshold. Our study showed that until the maximum pulse intensity achieves the threshold value, no energy losses occur and the pulse power does not change. Only after the achievement of the threshold intensity, multiphoton ionisation appears and the pulse power and intensity decrease and multiphoton ionisation ceases. As a result, the filamentation process ends, although the pulse power still exceeds the critical value. This circumstance demonstrates the influence of the pulse spectrum considered in the Bespalov – Talanov theory on the type of filamentation development. Thus, the type of the process substantially depends on the features of the spatial intensity distribution in the pulse. A distinct feature of our paper is that we consider the influence of the pulse spectrum on the evolution of filaments. In particular, we investigated in detail the evolution of a solitary pulse at the initial stage of the process.

At present four institutes in France and Germany are engaged in the Teramobile project on the experimental and numerical investigation of the propagation of high-power femtosecond pulses. In experiments with terawatt pulses, a few tens of filaments were observed which formed clusters of length exceeding ten metres. The numerical simulation of the real experimental problem can be performed only by using parallel calculations.

The filamentation process was mathematically simulated

A.D. Balashov, A.Kh. Pergament M.V. Keldysh Institute for Applied Mathematics, Russian Academy of Sciences, Miusskaya pl. 4, 125047 Moscow, Russia; e-mail: anbal@yandex.ru

Received 24 January 2006; revision received 18 May 2006
Kvantovaya Elektronika **36** (9) 825 – 834 (2006)
Translated by M.N. Sapozhnikov

in many papers [6–9]. Usually, a nonstationary three-dimensional system of equations for the slowly varying light-field amplitude was considered. To compare experimental data with the results of calculations taking into account small-scale perturbations, it is necessary to use approximately 10^{16} calculation cells. This requires a long time for the numerical solution of equations at long distances. To study the formation of filaments and their ordering to clusters qualitatively, a simplified physical model is used for calculating the propagation of a high-power laser pulse over long distances for an acceptable time by applying the method of parallel calculations.

2. Physical model and its averaging

The propagation of short pulses in a medium with the cubic nonlinearity is usually described by the system of equations [6] consisting of the nonlinear Schrödinger equation (NSE) for the electric-field envelope $E(X, Y, Z, t)$ moving at the group velocity v_g (here, Z is the coordinate along which the pulse propagates and XY is the plane perpendicular to the pulse propagation direction),

$$\frac{\partial E}{\partial Z} = \frac{\mathrm{i}}{2k_0}\nabla_\perp^2 E - \mathrm{i}\frac{k''}{2}\frac{\partial^2 E}{\partial t^2} + \mathrm{i}k_0 n_2 R(t)E - \left(\frac{\sigma}{2} + \mathrm{i}\frac{k_0}{2\rho_{\mathrm{cr}}}\right)\rho E - \frac{\beta^{(K)}}{2}|E|^{2K-2}E, \quad (1a)$$

where

$$R(t) = (1-\theta)|E|^2 + \frac{\theta}{\tau_K}\int_{-\infty}^{t}\exp\left(\frac{t-t'}{\tau_K}\right)|E(t')|^2\mathrm{d}t', \quad (1b)$$

and the equation describing the Drude model [10] for the local plasma density $\rho(X, Y, Z, t)$,

$$\frac{\partial \rho}{\partial t} = \sigma_K \rho_{\mathrm{nt}}|E|^{2K} + \frac{\sigma}{U_{\mathrm{i}}}\rho|E|^2, \quad (1c)$$

where $k_0 = 2\pi/\lambda_0$ is the central wave number ($\lambda_0 = 800$ nm is the central wavelength); $n_2 = 3.1 \times 10^{-19}$ cm^2 W^{-1} is the nonlinear refractive index caused by the Kerr effect; $k'' = 0.2$ fs^2 cm^{-1} is the group-velocity-dispersion coefficient; $\tau_K = 70$ fs is the relaxation time; $\rho_{\mathrm{cr}} = 1.8 \times 10^{21}$ cm^{-3} is the critical plasma density; $\beta^{(K)} = 4.25 \times 10^{-98}$ cm^{13} W^{-7} is the multiphoton absorption coefficient; $K = 8$ is the number of photons required for the ionisation of oxygen molecules having a higher ionisation potential than nitrogen molecules for which $K = 10$; $\sigma = 5.44 \times 10^{-20}$ cm^2 is the coefficient of cascade ionisation and plasma absorption in the cross section for inverse bremsstrahlung; $\sigma_K = 2.88 \times 10^{-99}$ cm^{16} s^{-1} W^{-8} is the multiphoton ionisation coefficient; $U_{\mathrm{i}} = 12.1$ eV is the ionisation potential of oxygen molecules; $\rho_{\mathrm{nt}} = 5.4 \times 10^{18}$ cm^{-3} is the effective density of neutral molecules equal to 20 % of the standard density $\rho_{\mathrm{at}} = 2.7 \times 10^{19}$ cm^{-3}. The parameter θ for simulating femtosecond pulses is set equal to 0.5, which allows us to take into account the term responsible for polarisation of molecules.

To reduce the calculation time, we can study qualitatively the propagation of high-power pulses in real laser systems by using the algorithm for simplifying the model proposed in [6]. First, because the influence of inverse bremsstrahlung for pulses shorter than a picosecond is negligible, we set $\sigma = 0$ (the recombination of electrons in the kinetic equation for the local plasma density is neglected). We will also neglect the time dependence of the second derivative $\partial^2 E/\partial t^2$ because the complex amplitude of the light wave slowly varies with time. Second, by assuming that intense light fields have Gaussian temporal profiles, we will seek the solution of the system of equations in the form of the product

$$E(X, Y, Z, t) = \psi(X, Y, Z)\exp\left[-\frac{(t-t_{\mathrm{c}})^2}{T^2}\right],$$

where $t_{\mathrm{c}}(Z)$ is the temporal layer where a peak with the maximal intensity and the half-width T is formed, which is preserved during the entire propagation time [6].

Taking into account the assumptions made above, we find first ρ from Eqn (1c):

$$\rho \simeq \left(\frac{\pi}{8K}\right)^{1/2} T\sigma_K \rho_{\mathrm{nt}}|\psi|^{2K} \times\left[1 + \mathrm{erfc}\left(\frac{(2K)^{1/2}[t - t_{\mathrm{c}}(Z)]}{T}\right)\right], \quad (2)$$

where

$$\mathrm{erfc}\, u = \frac{2}{\sqrt{\pi}}\int_0^u \exp(-s^2)\mathrm{d}s.$$

Then, we substitute ρ and expression (1b) into (1a), multiply the obtained equation by $\exp[-(t-t_{\mathrm{c}})^2/T^2]$ and integrate over the entire temporal domain, i.e. from $-\infty$ to $+\infty$. After some simplifications, we obtain

$$\frac{\partial \psi}{\partial Z} = \frac{\mathrm{i}}{2k_0}\nabla_\perp^2\psi + \mathrm{i}k_0 n_2 \alpha|\psi|^2\psi - \mathrm{i}\gamma|\psi|^{2K}\psi - \frac{\beta^{(K)}}{2\sqrt{K}}|\psi|^{2K-2}\psi, \quad (3)$$

where

$$\alpha = \frac{1}{\sqrt{2}}\left(1 - \theta + \frac{\theta D}{\sqrt{2}\tau_K}\right);\quad \gamma = \left(\frac{\pi}{8K}\right)^{1/2}\frac{k_0 T\sigma_K\rho_{\mathrm{nt}}}{2\rho_{\mathrm{cr}}};$$

$$D = \int \exp\left(-\frac{T^2}{8\tau_K} - \frac{u}{\tau_K} - \frac{2u^2}{T^2}\right) \times\left[1 + \mathrm{erfc}\left(\frac{u\sqrt{2}}{T} - \frac{T}{\sqrt{8}\tau_K}\right)\right]\mathrm{d}u.$$

In [11], the influence of Raman scattering on a nonlinear response in air at $\theta = 1/2$ was demonstrated. Let us assume that $T = 0.1t_{\mathrm{p}}$ (where t_{p} is the pulse duration) for the filamentation process in the presence of multiphoton ionisation, which reduces the pulse duration. Let us introduce dimensionless variables

$$z = Z\left[\frac{(\alpha k_0 n_2)^K}{\gamma}\right]^{1/(K-1)},\quad x = X(2k_0)^{1/2}\left[\frac{(\alpha k_0 n_2)^K}{\gamma}\right]^{1/(2K-2)},$$

$$y = Y(2k_0)^{1/2}\left[\frac{(\alpha k_0 n_2)^K}{\gamma}\right]^{1/(2K-2)},$$

the field

$$A = \psi\left(\frac{\gamma}{\alpha k_0 n_2}\right)^{1/(2K-2)}$$

and the parameter

$$v = \frac{\beta^{(K)}}{2\sqrt{K}}\left(\alpha k_0 n_2 \gamma^{K-2}\right)^{1/(K-1)}$$

into Eqn (3) to obtain after some simplification

$$\frac{\partial A}{\partial z} = \mathrm{i}\nabla_\perp^2 A + \mathrm{i}|A|^2 A - \mathrm{i}|A|^{2K} A - v|A|^{2K-2} A, \qquad (4)$$

where $v = 0.154$ for the parameters t_p and T selected above.

Equations of the NSE type can be numerically simulated by various methods which reduce the calculation time by preserving the required calculation accuracy.

The spectral method allows one to use the fast Fourier transform algorithm, but it can be realised only on uniform networks. The advantage of the spectral method is obvious only for simple solutions of the moving soliton type.

The splitting over processes is performed as follows: the solution of Eqn (4) on the interval Δz is replaced by the successive solution of two-dimensional diffraction problems in a linear medium first in planes parallel to the plane xz and then in planes parallel to the plane yz. Then, the nonlinear phase shift of the light field is calculated on the same interval Δz in the absence of diffraction. For the schemes of splitting over processes, the problem of conservation is important, which requires a separate discussion.

In this paper, a direct method for solving Eqn (4) was used, i.e. the implicit conservative difference scheme was constructed and then the Newton method was applied. The propagation of a laser pulse is usually simulated by using the initial pulse profile in the form

$$A(z=0) = \sqrt{I_0}\exp\left[-\frac{\left(x^2+y^2\right)^N}{w_0^{2N}}\right], \qquad (5)$$

where w_0 and $\sqrt{I_0}$ are the dimensionless initial width and amplitude of the pulse. The power N is usually set equal to unity (Gaussian pulse) or two (super-Gaussian pulse).

3. Study of the nonlinear stage of the Bespalov – Talanov instability

The theory of formation of the filament structure of a light beam due to self-focusing was first developed by Bespalov and Talanov in 1966 [12]. They showed that the amplitude – phase perturbations of a plane electromagnetic wave in a nonlinear dielectric lead to its decay into individual beams having different self-focusing lengths depending on the scale of the initial perturbation. To find this dependence, we study the solution of the NSE in the form of a plane wave

$$A = (A_0 + a)\exp(\mathrm{i}|A_0|^2 z),$$

where $A_0 = \mathrm{const}$ is the unperturbed wave amplitude and $|a| \ll A_0$. By studying the stability problem in the linear approximation, we have

$$a \sim \exp(-\mathrm{i}\boldsymbol{k}_\perp \boldsymbol{r}_\perp - \mathrm{i}hz),$$

where $\boldsymbol{k}_\perp$ and $\boldsymbol{r}_\perp$ are the projections of the wave vector $\boldsymbol{k}$ and radius vector $\boldsymbol{r}$ on the plane xy. Then, the development of perturbations can be determined depending on the value of $k_\perp$ (Fig. 1).

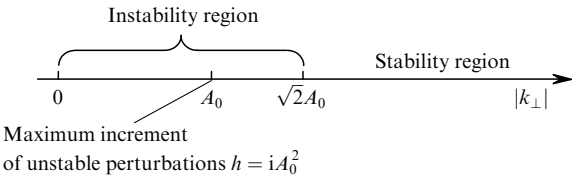

Figure 1. Dependence of the type of perturbations on $k_\perp$.

The numerical simulation of the results obtained by Bespalov and Talanov presents no problems but is important for substantiating some features of the pulse propagation. Due to the fundamental nature of these results, we consider once more in detail the numerical simulation of the Bespalov – Talanov instability, in particular, the simulation of the nonlinear stage of the process.

Consider the one-dimensional case of Eqn (4) by neglecting ionisation effects. The initial perturbation is specified in the form

$$A(x,0) = 20 + 2\cos(k_\perp x),$$

i.e. $A_0 = 20$. Calculations were performed for different values of $k_\perp$ and completely confirmed the theory presented above. Figure 2 shows the behaviour of the maximum value of the modulus of the solution $\max_x |A(x,z)|$ for different regimes. If the wave-vector modulus $|\boldsymbol{k}_\perp| \equiv k_\perp$ is large enough (i.e. $k_\perp > \sqrt{2}A_0$), the solution is stable and periodically changes [curve (*1*) in Fig. 2]. The value $k_\perp = \sqrt{2}A_0$ is the stability boundary, and the solution for such $k_\perp$ does not change along z [curve (*2*)]. If $k_\perp < \sqrt{2}A_0$, the solution increases exponentially with z. In this case, it remains harmonic in x at the initial stage. As z increases, the solution is no longer harmonic in x (Figs 3a, b). Thus, as expected, only the initial stages of the instability correspond to the exponential increase [curves (*3–5*) in Fig. 2]. Curve (*4*) in Fig. 2 corresponds to the

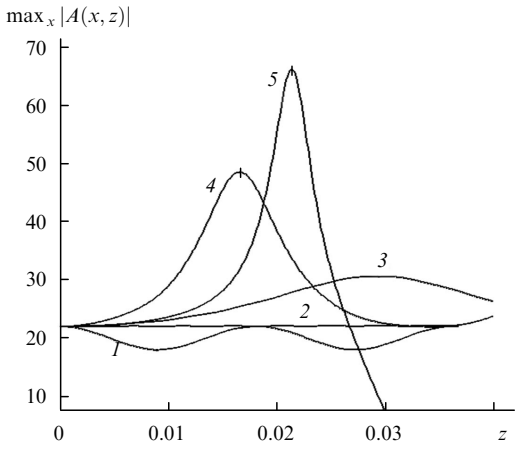

Figure 2. Dependences of the maximum value of the modulus $\max_x |A(x,z)|$ of the solution on the distance z for $k_\perp = \sqrt{3}A_0 > \sqrt{2}A_0$ (*1*), $\sqrt{2}A_0$ (*2*), $(1+\sqrt{3}/2)^{1/2}A_0 < \sqrt{2}A_0$ (*3*), A_0 (*4*), $(1-\sqrt{3}/2)^{1/2}\times A_0 < A_0$ (*5*). The vertical bars on curves (*4*) and (*5*) correspond to distances z for which the distributions $|A(x,z)|$ are presented in Figs 3a and b, respectively.

fastest development of instability, when the increment of unstable perturbations is maximal ($h = iA_0^2$).

Figures 3a, b show the distributions of perturbations in the initial state for $z = 0$ and other $z > 0$ corresponding to the vertical bars on curves (*4*) and (*5*) in Fig. 2. In Fig. 3a the minimal distance on which the instability develops is 0.016, and in Fig. 3b this distance is 0.021 (perturbations develop not so rapidly).

The picture of the development of periodic perturbations described above is also preserved as a whole in the two-dimensional case [13]. Note that the Bespalov–Talanov theory concerns only the initial stage of the development of perturbations. Upon simulation of stable periodic perturbations at larger distances, a considerable increase in the amplitude also occurs. Figure 3c presents the distribution of stable perturbations according the Bespalov–Talanov theory ($k_\perp = \sqrt{3}A_0 > \sqrt{2}A_0$), but unlike Fig. 3a, simulation was performed at larger distances. The type of the solution considerable changes and numerous rapidly increasing maxima appear, i.e. stable modes at the nonlinear stage can give rise to unstable structures (filaments).

Aside from the harmonic perturbation, we also considered the evolution of a single perturbation. It is known [5] that filamentation develops at a certain power of the beam. However, the dynamics of this process was not considered in most papers. It is shown in our paper that this process depends considerably not only on the pulse power but also on its spectrum. The perturbation was described by a Gaussian beam, i.e. the initial condition had the form

$$A(r, 0) = A_0 + a_0 \exp\left(-\frac{r^2}{w_0^2}\right).$$

In this case, the solution represents a solitary maximum up to a certain distance z: the subsequent decay of the maximum is not considered. If the pulse width w_0 is small, this means that the beam has a broad spectrum, and if the fraction of low-frequency components (which exponentially increase according to the Bespalov–Talanov theory) is small, the amplitude of such a beam at the linear stage of instability will not increase. Under such initial conditions, the beam first broadens and its amplitude decreases. Indeed, first the widths of beams with $w_0 = 0.05$, 0.08, and 0.11 increase (Fig. 4b) and their amplitudes decrease (Fig. 4a).

To study the solitary maximum, we write the Fourier transform for the function $A(r, 0) = A_0 \exp(-r^2/w_0^2)$:

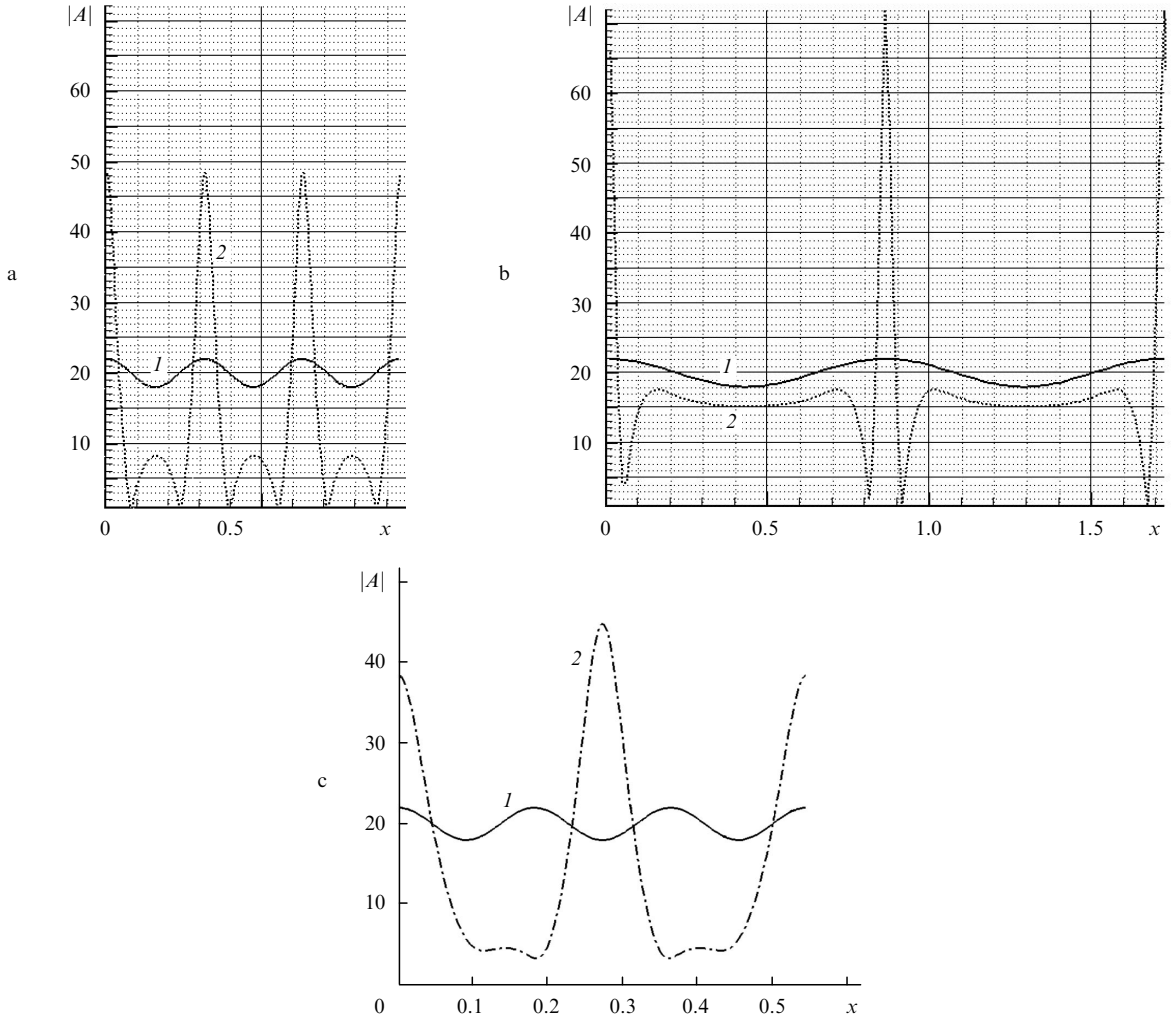

Figure 3. Distributions of the amplitudes $|A|$ for z = 0 (*1*) and $z > 0$ (*2*) for $k_\perp = A_0$ (corresponds to the maximum increment of the development of perturbations) (a) $k_\perp = (1 - \sqrt{3}/2)^{1/2}A_0 < A_0$ (b), and $k_\perp = \sqrt{3}A_0 > \sqrt{2}A_0$ (c). The development of instability in Fig. 3c occurs in the nonlinear phase.

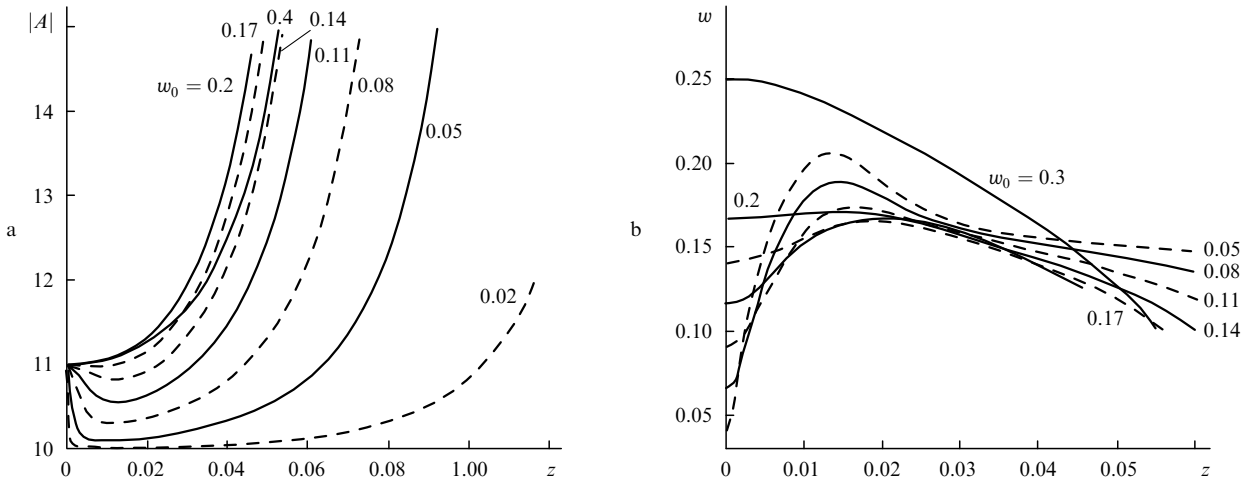

Figure 4. Changes in the field amplitude $|A|$ on the axis (a) and the width w of the beam profile (b) or $A_0 = 10$ and $a_0 = 1$ and different values of w_0.

$$\exp\left(-\frac{r^2}{w_0^2}\right) = \frac{1}{(2\pi)^2}\int_{-\infty}^{+\infty}\varphi(\boldsymbol{k})\exp(\mathrm{i}\boldsymbol{kr})\mathrm{d}k_x\mathrm{d}k_y,$$

where

$$\varphi(\boldsymbol{k}) = \int_{-\infty}^{+\infty}\exp\left(-\frac{r^2}{w_0^2}\right)\exp(-\mathrm{i}\boldsymbol{kr})\mathrm{d}x\mathrm{d}y$$

$$= \pi w_0^2\exp\left[-\frac{w_0^2}{4}\left(k_x^2+k_y^2\right)\right],$$

i.e.,

$$A(r,0) = A_0\exp\left(-\frac{r^2}{w_0^2}\right) = \frac{A_0 w_0^2}{4\pi}$$

$$\times\int_{-\infty}^{+\infty}\exp\left[-\frac{w_0^2}{4}\left(k_x^2+k_y^2\right)\right]\exp[\mathrm{i}(k_x x+k_y y)]\mathrm{d}k_x\mathrm{d}k_y$$

is the expansion of the initial perturbation into the superposition of the considered waves. The smaller w_0, the broader the signal spectrum and the smaller its fraction in the region of small k [here, $k = (k_x^2+k_y^2)^{1/2}$], i.e. for small w_0 the signal will increase faster than for large w_0. However, such an initial perturbation is unstable as a whole because the values of k satisfying the Bespalov–Talanov condition always exist.

If the initial width of the beam is large enough, the beam amplitude increases and its width decreases because the fraction of the low-frequency growing components of the spectrum is large. For Gaussian beams, the spectral distribution is also Gaussian, the greater part of the spectrum being located in the region $k \leqslant 2/w_0$. For this part of the spectrum to satisfy the Bespalov–Talanov conditions, the inequality $2/w_0 \leqslant \sqrt{2}A_0$ should be fulfilled, i.e. $w_0 \geqslant \sqrt{2}/A_0$. In the given case, $w_0 > 0.14$ because $A_0 = 10$. Our calculations showed that up to $w_0 \approx 0.17$ the beam amplitude first decreases and its width increases. Further, at the nonlinear stage such beams will behave as broader beams, but at larger z.

During the development of instability, the parts of the spectrum where $k > \sqrt{2}A_0$ are suppressed and the beam broadens, i.e. the spectrum with small k narrows down (Fig. 4, $w_0 < 0.2$). Thus, as the beam broadens, the high-frequency components satisfying the stability condition decay, thereby increasing the contribution to the decay of low-frequency (unstable) components (this occurs due to the conservation of the first integral corresponding to the total beam power).

However, important is the dependence of the spectrum not only on the instability boundary but also on the maximum increment region. As w_0 is further increased, the spectrum continues to narrow down and, hence, the increasing number of the wave numbers k will be smaller than A_0, which corresponds to a slower development of instability (Fig. 4, $w_0 = 0.2$ and 0.4). In this case, stable components are absent and, therefore, the beam is not broadened.

4. Calculation for a single Gaussian pulse

Consider the solutions of Eqn (4) taking into account multiphoton ionisation. The results will be often interpreted by using dimensionless parameters.

Figure 5 shows the dependences of power P on the distance z for the high initial power of a Gaussian beam close to the threshold (or maximal) and the power slightly exceeding the critical power P_{cr}. Note that the propagation of laser pulses was simulated in many papers by characterising them only by their power as the parameter determining the type of propagation. However, this can be sometimes

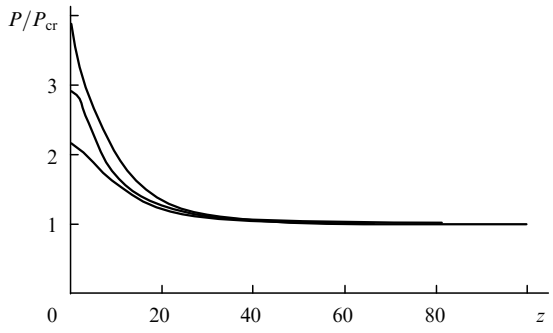

Figure 5. Dependence of the power P on the distance z for different initial beam powers.

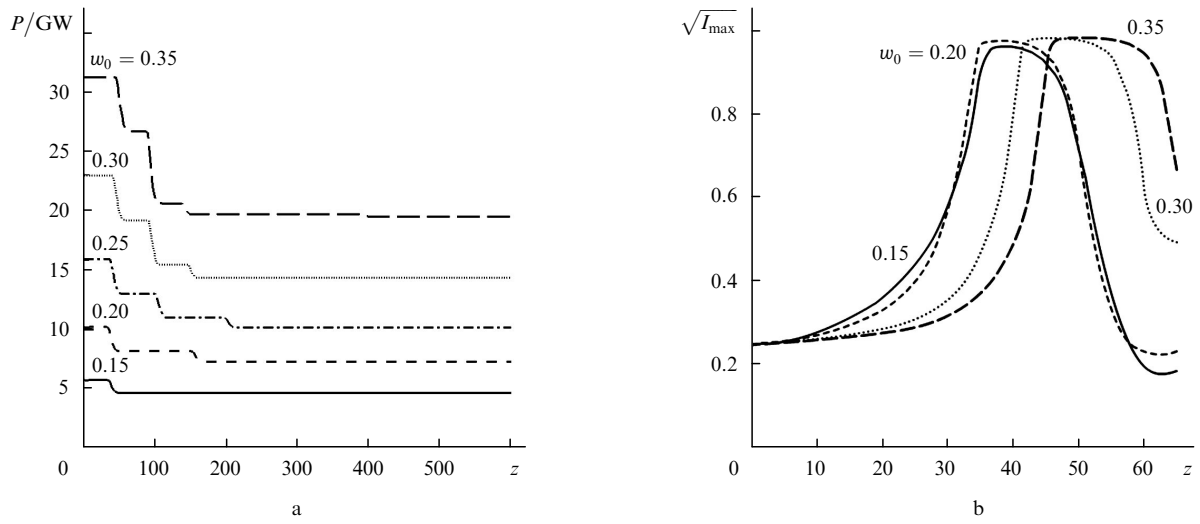

Figure 6. Dependences of the beam power (a) and peak intensity (b) on the distance z for $\sqrt{I_0} = 0.25$ for different initial pulse widths w_0.

insufficient for revealing in full measure the pulse propagation properties, and the initial width and maximum intensity of the pulse should be also taken into account. The type of propagation of a laser pulse can considerably depend on the combination of these parameters at the same critical power.

Figure 6 presents the dependences of the power and maximum amplitude $\sqrt{I_{\max}}$ on the distance z for Gaussian pulses with the same initial amplitude $\sqrt{I_0} = 0.25$ and different initial widths w_0. One can see (Fig. 6b) that the rate of increase in the peak intensity depends not only on the pulse power (for $P < P_{\rm cr}$, defocusing occurs) but also on its width.

The increase of the pulse intensity in the problem under study is limited by plasma effects and, as follows from Fig. 6, the maximum intensity does not exceed unity. The dimensional maximum intensity is $\sim 7 \times 10^{13}$ W cm^{-2}, in accordance with experimental data. As the radiation intensity increases, the last term in Eqn (4) responsible for multiphoton absorption begins to play an increasing role. Thus, as follows from Fig. 6a the pulse intensity drastically decreases. At the same time, the influence of another term in this equation responsible for multiphoton ionisation increases. This term reduces the action of the Kerr effect. Due to absorption of radiation during multiphoton ionisation and defocusing, the peak intensity of the pulse decreases, resulting in the ceasing of multiphoton ionisation and a constant value of the power integral up to the next instant of the intensity increase.

The Hamiltonian

$$H = \int\int \left(|\nabla_\perp A|^2 - \frac{|A|^4}{2} \right) {\rm d}x{\rm d}y$$

changes its sign to positive by the time of the establishment of a constant power level (Fig. 6a), which is the necessary condition for the beam divergence on the average [14]. However, the presence of divergence does not contradict the fact that an internal part of the beam can be focused. The further development of the beam profile can be analysed by using the Bespalov–Talanov theory. For this purpose, we consider the spectrum of the spatial distribution of the field A at a large enough distance z (Fig. 7).

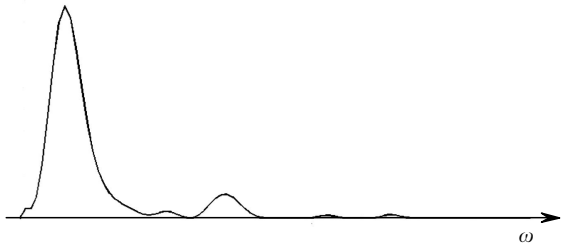

Figure 7. Spatial distribution spectrum of the field A.

Recall [12] that the instability increment plays an important role only in the case if the pulse spectrum contains harmonics that are smaller than the average value of the distribution $\mathrm{Re}\,\psi$, which is almost zero for large z. Therefore, from the point of view of the Bespalov–Talanov instability, the further development of unstable perturbations is impossible.

To explain the stepwise decrease in the pulse power, we consider in more detail the stages of self-focusing of a Gaussian pulse described in [13]. As mentioned above, the Gaussian pulse self-focusing requires the concentration of low frequencies of the spectrum. If the beam width is large, the fraction of low-frequency components is also large and self-focusing occurs without the initial broadening of the pulse, unlike the case of less broad pulses. As a result, a rather steep intensity 'column' is formed surrounded by a background produced by a defocused part of the initial pulse (Fig. 8a). However, once the peak intensity achieves the threshold value, it begins to decrease due to ionisation losses and the defocusing action of the electron plasma produced upon multiphoton ionisation. The first regions subjected to the action are regions of large gradients. In the case under study, the intensity decreases faster at the edge of the 'column' (Fig. 8b).

As the intensity further decreases, the power outflow from the centre meets the replenishment regions and a quasi-stationary annular structure is formed (Fig. 8c). Figure 9 (corresponding to Fig. 8b) shows power flows determined by the phase gradient $\varphi(x, y) = \arctan(\mathrm{Re}A/\mathrm{Im}A)$. The three structures can be distinguished in the figure: the central near-axis profile and two annular structures. The

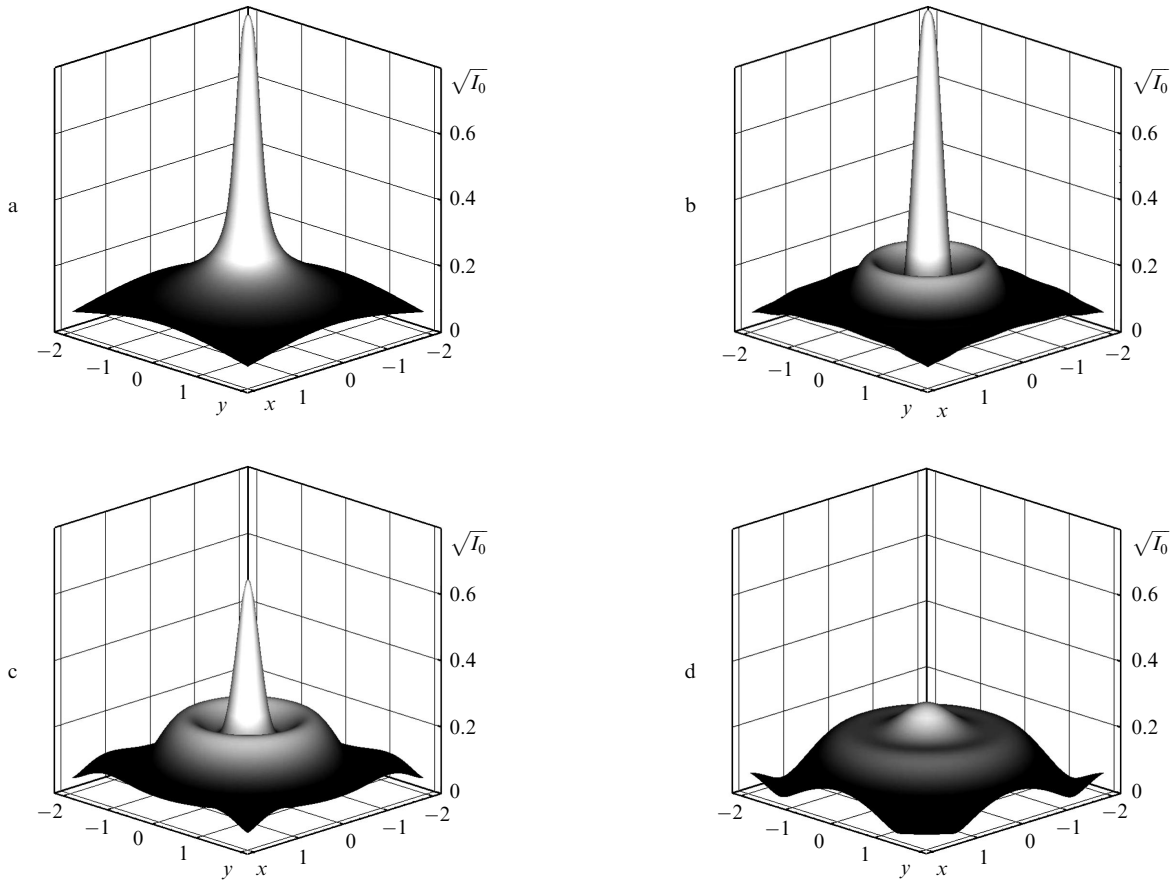

Figure 8. Distributions of the amplitude $\sqrt{I_0}$ for $z = 37.6$ (a), 45.4 (b), 54.7 (c) and 85.9 (d).

power flow inside these structures is directed to the centre. The structures are separated by the regions with the minimum intensity (dark regions), where the power flow is directed from the centre.

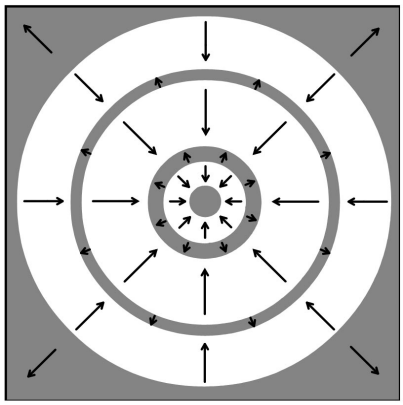

Figure 9. Phase gradient of the complex quantity $A(x, y)$. Directions of the power fluxes are indicated by the arrows.

When a certain power is concentrated in the annular structure after a decrease of the intensity 'column', the conditions are produced for a repeated increase of the 'column'. In the case under study, such a condition is the distribution shape (Fig. 8d) – a Gaussian profile with the power above the critical value and the half-width sufficient for the development of self-focusing. Thus, the intensity first increases, the annular structure is formed, and after the decrease in the intensity the profile is formed which experiences self-focusing again. As a result, the pulse power decreases stepwise (Fig. 6a).

The type of variation in power presented in Fig. 5 can be explained by the absence of the background of low-frequency spectral components around the pulse. Therefore, it is necessary to begin the simulation of pulse propagation from the time of laser pulse entering into a nonlinear medium rather than from the self-focusing development stage. Note also that the establishment of a constant power level (Fig. 6a) only means that this level is preserved up to some value of z because, as discussed above, filamentation can occur at large distances in the case of stable perturbations (Fig. 3c).

Figure 10 shows the decrease in the pulse power P and increase in its peak intensity $I_{\max}$ at the pulse propagation length z. One can see that absorption begins at the threshold intensity $I_{\text{th}} \approx 0.7$. According to the estimate performed in [15], the ionisation of air becomes significant at the intensity of 4.5×10^{13} W cm^{-2}, which corresponds to the dimensionless threshold found. As the pulse power decreases, the power loss and length at which absorption is observed decrease.

Let us write the equation for the dependence of the pulse power on the coordinate z. For this purpose, we multiply Eqn (4) by A^* and add the result with the equation complex conjugate to (4) and multiplied by A. By integrating over the entire transverse plane xy, we obtain

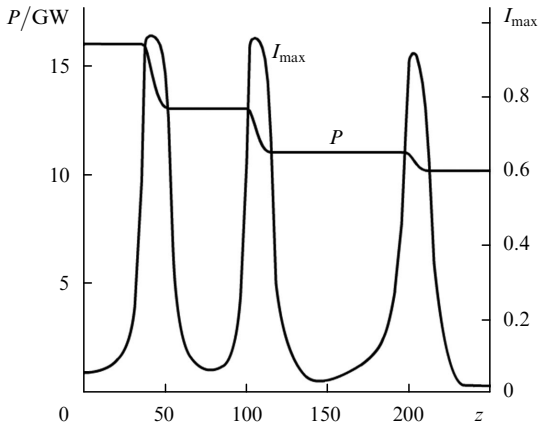

Figure 10. Dependences of the intensity I_{max} and power P on the distance z.

$$\frac{\partial P}{\partial z} \equiv \frac{\partial}{\partial z}\int |A|^2 \mathrm{d}x\mathrm{d}y = -2v\int |A|^{2K}\mathrm{d}x\mathrm{d}y \approx -2vK^{-1/N}P,$$

$$P_{cr} \approx P_0 \exp(-2vK^{-1/N}\Delta z_d) \approx P_0(1 - 2vK^{-1/N}\Delta z_d).$$

The approximate equality was obtained by using the expression for the initial shape of the pulse. Thus, we can estimate the length of the dissipative region as

$$\Delta z_d = \frac{K^{1/N}}{2v}\left(1 - \frac{P_{cr}}{P_0}\right),$$

which tends to ~ 0.25 for $N \to 1$ and $P_0 \gg P_{cr}$, which is confirmed by the results of calculations presented above. In the dimensional units, we have $\Delta z_d \approx 0.35$ m.

The stepwise variation of the pulse power also depends on its initial width. Figure 11 shows variations in the pulse power for pulses with the same initial power.

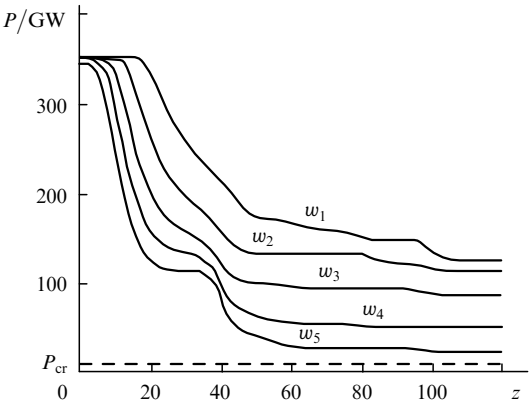

Figure 11. Dependences of the power on z for different initial pulse widths ($w_1 > w_2 > w_3 > w_4 > w_5$) and the same initial power.

5. Calculation for two Gaussian pulses

We have already considered the mutual influence of two Gaussian pulses in paper [13]. This influence becomes more noticeable in the case of multiphoton ionisation. The simulation of the mutual influence of two pulses performed by the research group headed by Kandidov was reported in [16], where the conditions restricting the power of pulses and the distance between them at which the interaction between pulses is possible were obtained. However, as in many other papers, the authors of [16] did not give due attention to the influence of the relation between pulse widths and intensities on the features of the phenomenon studied, although these relations can be considerably different at the same powers. In addition, the interaction between the high-intensity regions of pulses was not clearly demonstrated and the question about the time of beginning of the interaction was not considered [16].

Let us present two examples of calculations of two Gaussian profiles demonstrating how the presence of dissipation influences the type of variation of high-intensity regions. We considered two identical Gaussian perturbations with the initial width $w_0 = 5$ and the amplitude $\sqrt{I_0} = 0.9$ separated by the distance $d = 15$ between their centres (Fig. 12). One can see that in the conservative case (Fig. 12a), i.e. for $v = 0$ in (4), the pulse power is concentrated and remains constant in the middle between the two perturbations. In the presence of dissipation ($v = 0.154$, Fig. 12b), each of the two pulses begins to lose its power, narrowing simultaneously, and the instant of their merging is located slightly farther over z than in the conservative case.

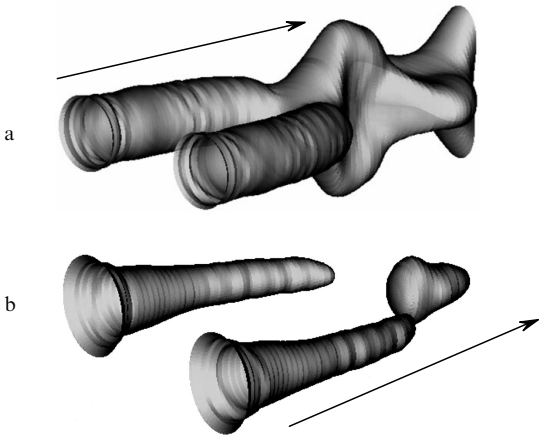

Figure 12. High-intensity regions for two identical Gaussian perturbations with $w_0 = 5$ and $\sqrt{I_0} = 0.9$ separated by the distance $d = 15$ between their centres in the absence of dissipation ($v = 0$) (a) and in its presence ($v = 0.154$) (b). The arrows indicate the propagation direction of the pulse.

The interaction between filaments in a broad pulse with power greatly exceeding the critical value is more complicated. Figure 13 shows qualitatively the power overflow from a developed filament with the maximum intensity to the region where a new filament is being produced.

6. Calculation for a high-power laser pulse

The development of parallel calculation methods [17], as a rule, makes it possible to calculate real physical systems. In the case of the propagation of a laser pulse over large distances, the use of parallel technologies is also justified. The aim of our paper is to prove the possibility of such a calculation.

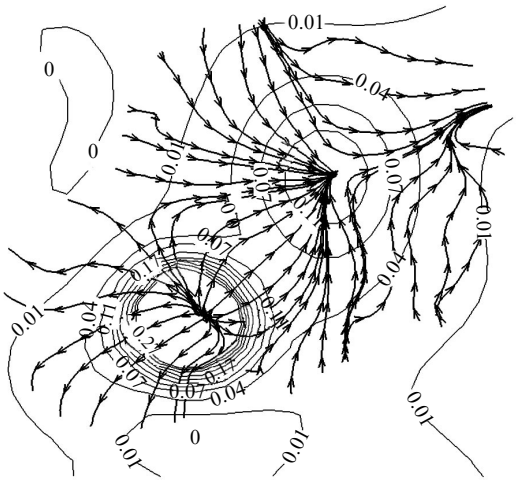

Figure 13. Power overflow between filaments in a broad beam (intensity level lines).

The power of a real laser pulse achieved a few terawatts and the pulse width is several centimetres. The pulse profile in real laser systems is usually represented by a super-Gaussian function, i.e. the exponent $N = 2$ in expression (5). The input profile of a real laser beam also contains noise. We reproduced a random field of amplitude fluctuations by the spectral method [18] based on the summation of the Fourier harmonics of the spatial spectrum.

The development of small-scale focusing [12] resulting in the decay of the profile symmetry is classically explained by the presence of amplitude fluctuations of the initial distribution. Due to small-scale self-focusing and the achievement of the multiphoton ionisation by the amplitudes of some fluctuations, multiple filamentation begins to develop in a high-power laser pulse. During this process, multiple connections are formed between individual filaments, resulting in the absorption and creation of new filaments. Such a chaotic development is accompanied by the formation of regions in laser pulses where filamentation occurs continuously due to the absorption of energy from adjacent regions. Such regions are called clusters [1], and the experimental data (Fig. 14) are explained by their presence.

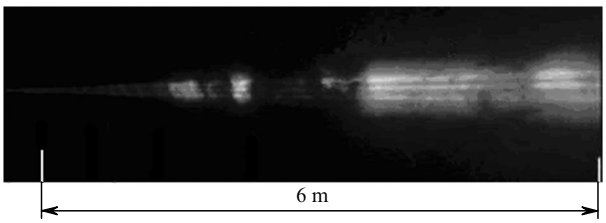

Figure 14. Experiment on the laser pulse propagation.

We will estimate the required dimensions of the calculation network from the following experimental conditions and data (Teramobile project [6]):

(i) The filamentation process is studied by using a high-power (100 GW – 3 TW) laser pulse with the initial width achieving 2 cm;

(ii) the width of filaments formed in experiments as a small-scale effect is constant and amounts to 100 – 150 μm, while the intensity at the filament focus can exceed the background intensity by tens of times;

(iii) the observed propagation length of the pulse is from tens to hundreds of metres.

Thus, the side of the square of the calculation network can achieve 10 cm to avoid a considerable influence of the network boundaries. The side of a cell should not exceed 10 – 15 μm in order to describe adequately small-scale effects. Therefore, the number of cells in the calculation region (xy plane) can achieve $10^4 \times 10^4 = 10^8$. A step in z decreases inversely proportional to the maximum intensity I_{max}, thereby providing not only stability but also the required accuracy of the solution. Due to a large dimensionality of the system of linear equations being solved and the necessity of numerical simulation of the propagation of a femtosecond pulse over large distances, we used a parallel calculation complex.

As an example we present the calculation for a pulse with an average power of $62P_{cr}$ and an initial width of 6 mm. The calculation region is a square with the side of length 2 cm. The Gaussian noise in the initial profile is specified by the algorithm described above. The calculation was performed by using the 2048×2048 network and the parallel calculation complex at M.V. Keldysh Applied Mathematics Institute, RAS.

The results of calculations of the intensity (Figs 15 and 16) and power (Fig. 17) of the pulse coincide with those obtained in the Teramobile project [6]. Moreover, the calculation rates of the parallel program complex developed for our work according to the Teramobile project are also comparable with those obtained in [6] despite the principle difference in the approach to the numerical solution of the problem. The approximation methods and characteristics of the parallel algorithm that we used are discussed in detail in [19]. As a rule, to obtain a high density of filaments, an elliptic distribution of the initial pulse profile is used in practice.

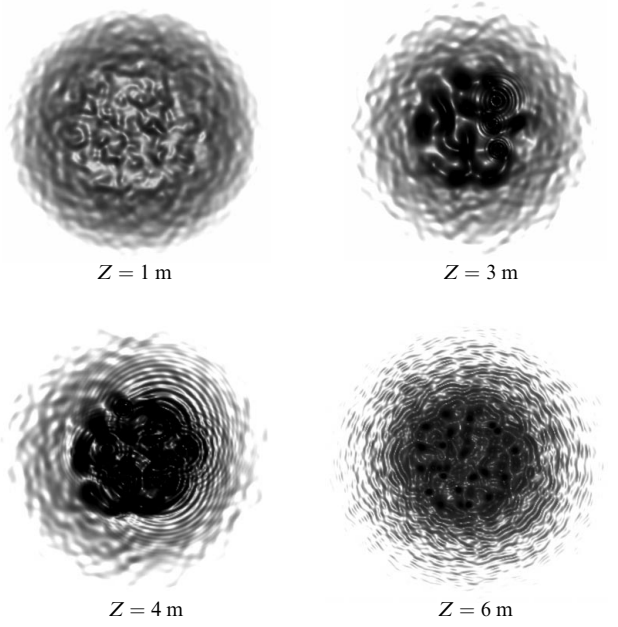

Figure 15. Intensity distributions for different Z.

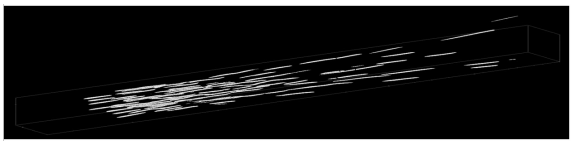

Figure 16. High-intensity regions during pulse propagation over the distance ~ 9 m.

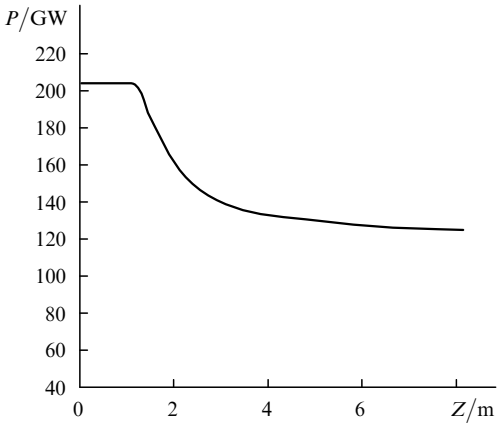

Figure 17. Dependences of the power P on the distance Z.

7. Conclusions

We have studied the filamentation process by numerical methods and developed the efficient algorithms for calculating filamentation in real laser systems. The symmetric difference schemes having the conservative nature were used and parallel programs for calculating such problems were developed.

It has been shown that the development of nonlinearity occurs stepwise and is determined by the threshold intensity 5×10^{13} W cm^{-2} at which the ionisation of air becomes considerable. The nature of the process is determined by the relation between multiphoton ionisation and small-scale focusing. Until the intensity achieves the threshold, the light beam does not lose its energy and self-focusing takes place. When the threshold is achieved, the energy losses appear due to ionisation and defocusing produced by the electron plasma, resulting in the intensity decrease. When the intensity becomes lower than the threshold value, self-focusing can begin again. Thus, the process has the stepwise nature. The process ceases when the spectrum of the pulse becomes such that the further development of instability in the linear approximation is impossible because the stability condition is fulfilled according to the Bespalov–Talanov criterion. However, the possibility of the regeneration of this process during the propagation of pulses over large distances has not been proved.

In the case of the initial Gaussian beam with a high intensity close to the threshold (or maximal) and power slightly exceeding the critical value, the stepwise variation in the intensity of the beam during its propagation was not observed.

References

1. Kasparian J., Rodrigues M., Mejean G., Yu J., Salmon E., Wille H., Bourayou R., Frey S., Andre Y.-B., Mysyrowicz A., Souerbrey R., Wolf J.-P., Woste L. *Science*, **61**, 301 (2003).
2. Braun A. et al. *Opt. Lett.*, **20**, 73 (1995); Nibbering E.T.J. et al. *Opt. Lett.*, **21**, 62 (1996).
3. Brodeur A. et al. *Opt. Lett.*, **22**, 304 (1997).
4. LaFontaine B. et al. *Phys. Plasmas*, **6**, 1615 (1999).
5. Chiao R.Y. *Phys. Rev. Lett.*, **13**, 5 (1964).
6. Skupin S., Berge L., et al. *Phys. Rev. E*, **70**, 046602 (2004).
7. Fibich G., Ilan B. *Phisica D*, **157**, 113 (2001).
8. Karamzin Yu.N., Sukhorukov A.P., Trofimov V.A. *Matematicheskoe modelirovanie v nelineinoi optike* (Mathematical Simulations in Nonlinear Optics) (Moscow: Moscow State University, 1989).
9. Volkov V.M. *Diff. Eq.*, **29**, 7 (1993).
10. Feit M.D., Fleck J.A. *Appl. Phys. Lett.*, **24**, 169 (1974).
11. Nibbering E.T.J., Grillon G., Franco M.A., et al. *J. Opt. Soc. Am. B*, **14**, 650 (1997).
12. Bespalov V.I., Talanov V.I. *Pis'ma Zh. Eksp. Teor. Fiz.*, **3**, 471 (1966).
13. Balashov A.D., Pergament A.Kh. Preprint M.V. Keldysh AMI, RAS, No. 40 (Moscow: 2004).
14. Landau L.D., Lifshits E.M. *Electrodynamics of Continuous Media* (Oxford: Pergamon Press, 1984; Moscow: Nauka, 1959).
15. Kasparian J., Sauerbrey R., Chin S.L. *Appl. Phys. B*, **71**, 877 (2000).
16. Kandidov V.P., Kosareva O.G., Shlenov S.A., et al. *Kvantovaya Elektron.*, **35**, 59 (2005) [*Quantum Electron.*, **35**, 59 (2005)].
17. Bukatov A.A., Datsyuk V.N., Zhegulo A.I. *Programmirovanie mnogoprotsessornykh vychislitel'nykh sistem* (Programming of Multiprocessor Calculation Systems) (Rostov-on-Don: Rostov State University, 2003).
18. Mirkin L.I., Rabinovich M.A., Yaroslavskii L.P. *Zh. Vych. Mat. Mat. Fiz.*, **5**, 1353 (1972).
19. Balashov A.D., Pergament A.Kh. *Mat. Model.*, **18**, 4 (2006).